IEEE Access
Multidisciplinary | Rapid Review | Open Access Journal

Received December 11, 2021, accepted January 10, 2022, date of publication January 20, 2022, date of current version February 2, 2022.

Digital Object Identifier 10.1109/ACCESS.2022.3144959

Adaptive Beamforming With Software-Defined-Radio Arrays

DANIEL CHRISTOPHER GAYDOS[1], PAYAM NAYERI[2], (Senior Member, IEEE), AND RANDY L. HAUPT[3], (Life Fellow, IEEE)

[1]Zeta Associates, Aurora, CO 80011, USA
[2]Electrical Engineering Department, Colorado School of Mines, Golden, CO 80401, USA
[3]Haupt Associates, Boulder, CO 80303, USA

Corresponding author: Payam Nayeri (payam_nayeri@ieee.org)

ABSTRACT Digital beamforming is the holy grail of antenna array technologies, however implementing digital beamforming into practical antenna arrays has been slow due to hardware complexity and cost. We propose a relatively inexpensive new approach to digital beamforming using software defined radios. Using this system, we carried out experiments on adaptive interference cancellation. We present detailed description of the beamformer system along with the developed control software and experimentally verify the beamformer performance. Our results show that in high-interference and high-multipath environments, where carrier frequency offsets cannot be measured, conventional interference cancellation algorithms fail. We propose two new robust solutions to this problem and compare the results with multiple techniques, including the minimum variance distortionless response beamformer, which outputs the highest possible signal-to-interference-plus-noise-ratio (SINR). We experimentally demonstrate that both our approaches work well in the face of these types of signal corruptions and are capable of interference cancellation without degrading SINR or other system performance factors, and without the need for transmitter and receiver synchronization.

INDEX TERMS Adaptive arrays, adaptive nulling, digital beamforming, interference cancellation, software-defined radio.

I. INTRODUCTION

Our wireless infrastructure and the spread of the Internet of Things (IoT) unleashed billions of radio-frequency (RF) devices that fill the allotted spectrum with signals. Signal interference, channel congestion, and noise in such environments challenge system designers [1], [2]. In order to survive the crowded and sometimes hostile radio spectrum, wireless communication and radar systems need to adapt and reconfigure to the environment in which they operate. Adaptive arrays dynamically weight and combine signals in a way that enhances the desired signal while rejecting interfering signals. Signal processing and optimization algorithms modify the element weights to enhance signal detection [3]–[6]. These arrays dramatically improve performance in hostile radio environments, but their very high cost limits implementation on a wide scale, particularly for civilian applications.

Until recently, the high cost of digital beamformers limited the number of hardware systems with full digital beamforming (DBF) capability [7], [8]. Hybrid beamforming approaches can help to reduce the cost of fully digital beamformers [9], with some limitations in performance. A single radio frequency channel digital beamforming array antenna based on compressed sensing was also proposed to reduce the hardware costs [10].

A cost effective solution for full DBF uses a direct conversion or zero intermediate frequency (IF) architecture. This architecture is commonly adopted in software defined radios (SDRs). SDRs provide a low-cost option for digital communication and can be used to increase the feasibility of DBF by placing an SDR at each element of an array. The SDRs convert the RF signal into digital data at the element level, enabling cost-effective DBF. Some beamforming experiments using SDR arrays have recently been reported, including direction finding (DF) and localization. SDR arrays have been used for DF in anechoic chambers [11], [12], and transmitter beam scanning [12], as well as source localization and array shape estimation [13]. Initial work on interference cancellation and adaptive nulling with SDRs have been reported in [14]–[17].

The associate editor coordinating the review of this manuscript and approving it for publication was Kuang Zhang.

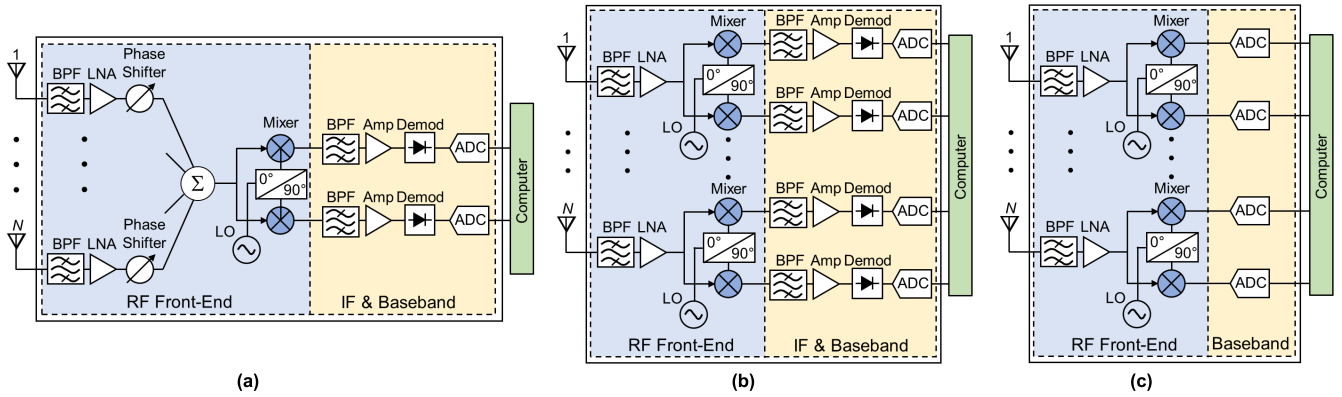

FIGURE 1. Simplified block diagrams of beamformer receivers. (a) Analog heterodyne. (b) Digital heterodyne. (c) Digital direct down-conversion.

On the other hand, practical implementation of DBF also requires robust algorithms for nonideal scenarios, which are commonly known as mismatched beamformers [4]. Robust algorithms have primarily focused on mismatches from steering vector errors, or finite sample size of the spatial spectral estimates [18]–[22]. A different category of beamformer mismatch is when the transmitter and receiver are not synchronized. Very limited work has been reported on robust approaches that account for signal corruptions arising from carrier frequency offsets [17], [23], [24]. However, in high-interference and high-multipath environments, typically measuring the carrier frequency offset is not feasible and robust solutions are needed.

The primary goals of this research are to, (1) build a low-cost platform for robust DBF using an array of SDRs, and (2) experimentally study the interference cancellation capability of the system in a realistic high-multipath environment. For experimental studies, we first used the developed four-element SDR digital beamformer to compare interference cancellation performance of conventional algorithms. We then show that in the case where the transmitter and receiver cannot be synchronized, these algorithms will fail. To overcome the shortcomings of these existing algorithms, we developed two new interference cancellation approaches. The first uses the conventional algorithms, but ignores signal phase, essentially performing an amplitude-only optimization of the array weighting vector. The second approach is based on a new interference cancellation error function and uses genetic algorithm (GA) for the optimization problem. Experimental results are presented, and we show that both proposed techniques provide robustness to this type of signal corruption in unsynchronized systems without degrading SINR or other system performance factors. In comparison between the two proposed techniques, the GA approach provides a higher SINR. We note that the initial results of this research were presented in [17]. In comparison, this extended version includes a description of the beamformer system architecture, a new direct calibration approach that outperforms the initial over-air technique, SINR studies along with description of the measurement approach, comparison with multiple beamforming algorithms, as well as experimental studies for synchronized and un-synchronized beamforming. In addition, multiple trials were conducted for each case study to verify the effectiveness of the algorithms. In short, the novelties and original contributions of this work are:

1. Experimental demonstration of a new cost-effective DBF platform using an array of SDRs, along with experimental studies on interference cancellation.
2. Development of two new interference cancellation solutions for unsynchronized transmitter-receiver communication systems along with experimental verification.

This paper is organized as follows. We introduce background on digital beamformer hardware architectures and adaptive nulling interference algorithms in section II. Section III provides details on the development of the proposed digital beamformer based on SDRs, discussing the hardware setup, calibration, and control algorithms. Experimental results on interference cancellation obtained using this testbed is given in Section IV, where we also highlight some shortcomings of the existing techniques. New interference cancellation algorithms that can operate without the need for synchronization are then given in Section V where we demonstrate the robustness of these techniques in a realistic high-multipath environment. This is followed by conclusions in Section VI.

II. PRELIMINARIES

A. SYSTEM ARCHITECTURES FOR ADAPTIVE BEAMFORMING

Fig. 1 (a) shows a diagram of an N-element active electronically scanning array (AESA) receiver. A reverse process exists for transmit in which the computer sends bits to a digital-to-analog converter (DAC) before modulating, amplifying, filtering, and up converting the signal [25]–[27]. At the receiver, the RF signal at each element gets phase shifted, then summed into one signal that is down converted. The IF stage filters and amplifies the single IF signal before demodulating it to a frequency that is compatible with the analog-to-digital converter (ADC) [28]–[32]. The computer

collects a reasonable amount of signal data. RF beamformers can perform low-resolution direction finding and blind adaptive nulling [5], [33], [34]. This AESA architecture converts all the RF data to a single digital output, so the signals at the element level are unknown. A basic architecture for a digital beamforming antenna array appears in Fig. 1 (b). Here, the signal at each element in the array down converts to an IF signal that passes to an ADC. For an N-element array, the computer receives N times as much data as the RF beamformer. The computer now has the ability to form the signal covariance matrix for high resolution DF or adaptive nulling [35]–[42].

This architecture is expensive, though. A cost effective solution to full digital beamforming is based on direct conversion or zero IF architectures. Direct down conversion (DDC) passes the RF signal from an element through a bandpass filter (BPF) and low-noise amplifier (LNA) before entering the ADC without the need of an IF stage. A basic architecture of a DDC receiver is given in Fig. 1 (c). Software defined radios commonly adopt this architecture. An SDR controls the transmit/receive waveform in software rather than hardware. Common hardware tasks, such as baseband modulation and coding, are performed in software as well [43]. SDR technology enables a radio to communicate at a desired frequency, bandwidth, modulation, and data rate through software changes rather than hardware changes.

B. ADAPTIVE NULLING ALGORITHMS

Array processing enhances the reception (or detection) of a desired signal in an environment containing numerous interference signals. Adaptive nulling algorithms place nulls in the directions of interference sources in order to maximize the system SINR. Consider the N-element linear array depicted in Fig. 2. The output signal, $y(t)$, is given by

$$y(t) = \boldsymbol{w}^T \boldsymbol{x}(t), \quad \text{where } \boldsymbol{x}(t) = \boldsymbol{s}(t) + \boldsymbol{n}(t). \tag{1}$$

Here $\boldsymbol{x}(t) = [x_1(t), x_2(t), \ldots, x_N(t)]$ is the input signal vector measured by the array, which has a signal, $\boldsymbol{s}$, and a noise, $\boldsymbol{n}$, component, $\boldsymbol{w} = [w_1, w_2, \ldots, w_N]$ is the array weighting vector, and the superscript T denotes transpose. The noise is assumed to be stationary and ergodic. Most adaptive nulling algorithms require a reference signal used for synchronization. The reference signal is denoted by d. The input signal vector, $\boldsymbol{x}(t)$, may be corrupted due to interference or other factors. The difference between these two signals defines the error vector:

$$\varepsilon(t) = d(t) - \boldsymbol{w}^T \boldsymbol{x}(t). \tag{2}$$

The expected value of the squared error in (2) is given by

$$E\left\{\varepsilon^2(t)\right\} = d^2(t) - 2\boldsymbol{w}^T \boldsymbol{r}_{xd} + \boldsymbol{w}^T \boldsymbol{R}_{xx} \boldsymbol{w}, \tag{3}$$

where $\boldsymbol{r}_{xd}$ is the signal covariance vector of the received and reference signals and $\boldsymbol{R}_{xx}$ is the covariance matrix of the received signals. Equation (3) defines the mean square error performance criterion and is a quadratic function of $\boldsymbol{w}$ whose extremum is a minimum.

Adaptive beamforming algorithms find a weighting vector to minimize (3). The most popular adaptive array beamformers is the minimum variance distortionless response (MVDR) beamformer which provides noise resilience while nulling interferers. The MVDR beamformer output has the highest possible SINR. When the covariance matrix of interference and noise is replaced by the sample matrix obtained the reference signal, the adaptive version of the MVDR beamformer is referred to as the sample matrix inversion (SMI) beamformer [44], [45]. As such, SMI serves as a benchmark reference for comparison with other beamforming algorithms and is adopted in our work. Other than SMI, the other best known algorithms include least mean square (LMS) and recursive least square (RLS) [4]–[6]. The LMS algorithm uses a gradient descent optimization. It loops over time samples and, for each time sample, it estimates a gradient vector based on that time sample and performs one step of a gradient descent optimization using the estimated gradient. Iterative numerical matrix inversion approaches help circumvent many computational problems. The RLS algorithm is a nonstationary iterative approach that weights recent time samples higher when computing an updated weighting vector. At iteration K, RLS attempts to minimize a weighted norm given by

$$\|\varepsilon\|_\alpha^2 = \sum_{k=-\infty}^{K} \varepsilon_k \alpha^k, \tag{4}$$

for some $0 < \alpha < 1$. RLS accounts for the past few samples in its computation of the array weighting vector.

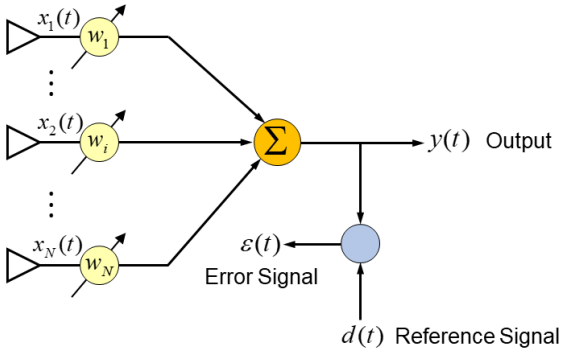

FIGURE 2. An adaptive array showing the setup of reference and error signals.

III. A SOFTWARE DEFINED RADIO DIGITAL BEAMFORMER

A basic block diagram of the beamformer with an SDR at each element is shown in Fig. 3. The computer controls beamforming using an interference cancellation algorithm, while the synchronization trigger and RF reference synchronize and calibrate the SDR array.

A. HARDWARE IMPLEMENTATION

Our experimental beamforming testbed has four National Instruments (NI) USRP 2922s which are programmable radio

transceivers [46]. The USRP (Universal Software Radio Peripheral) devices interface to the computer via an Ethernet switch. Each USRP provides an independent transmit and receive channel capable of full duplex operation, which acts as one array channel when the antenna is connected to the duplex transmit and receive port of the USRP. The SDR has a tunable center frequency from 400 MHz to 4.4 GHz and up to a 20 MHz instantaneous bandwidth with 16-bit sample width I/Q streaming at 25 MS/s for host-based processing with NI LabVIEW [47]. While these SDRs provide flexibility for frequency reconfiguration, our experimental setup functions at 2.45 GHz.

Our beamformer uses four monopole antenna elements, each connected to one USRP. The monopole antennas are placed 61 mm ($\lambda/2$ at 2.45 GHz) apart, on a custom-built 3D printed high-impact polystyrene mount. A photo of the monopole array is given in Fig. 4 (a). An OctoClock-G CDA-2990 clock distribution accessory synchronizes the SDRs for coherent beamforming [48]. This device has a 10 MHz and a 1 PPS timing source that synchronize the local oscillator (LO) frequencies and sample clocks at each SDR. An image of the four USRPs and synchronization clock is given in Fig. 4 (b). A computer running LabVIEW controls the beamformer. Fig. 4 (c) is a photo of the complete beamformer including the computer, SDRs, synchronization clock, and the antenna array.

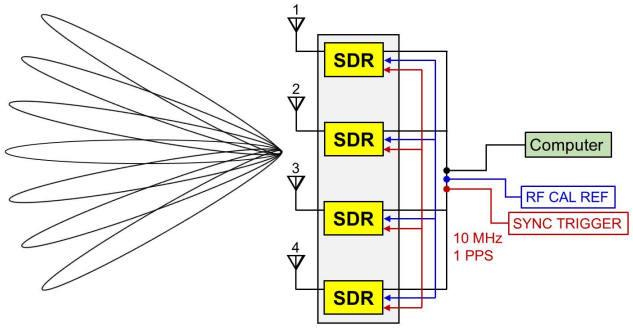

FIGURE 3. Simplified block diagram of the proposed SDR beamformer.

B. BEAMFORMER CALIBRATION

The commercial clock distribution accessory synchronizes the sample clocks and aligns the LO frequency but does not align the LO phase of each SDR device. As a result, phase ambiguities in the LOs prevent coherent beamforming. Calibrating the relative phases of the LOs and relative amplitudes of the SDRs can be done using a plane wave from an external transmitter as a reference signal inside an anechoic chamber [13]. However, this approach shows poor performance in realistic high-multipath environments [17]. An alternative approach sends a reference signal to each SDR over a cable connected to the SDR receive port through an RF switch or through a second receive port on the SDRs [11], [12]. The latter approach requires enough leakage between the two receive ports such that the reference signal at the second receive port is measured by the receive port connected to the array element. In our beamformer, each USRP has a duplex port (RX1/TX1) and a receive-only port (RX2). The duplex ports connect to the array elements and the receive-only ports connect to an RF reference signal from a Signal Hound VSG25A signal generator [49] through a custom four-way power divider shown in Fig. 5. The power divider uses three microstrip T-junctions, which does not isolate the output ports, so it relies on the SDRs' isolation between the RX2 port and RX1/TX1 port to prevent array signals from reaching the power divider outputs.

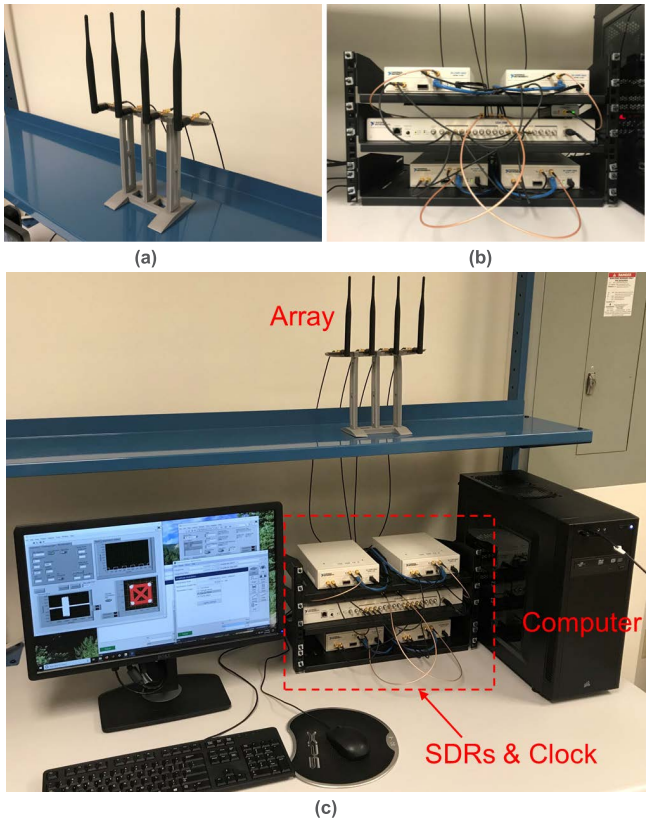

FIGURE 4. Hardware setup of the digital beamformer: (a) close-up of the four element monopole array on a custom 3D printed antenna mount, (b) close-up of the four SDRs (top and bottom shelves) and the synchronization clock (center shelf) on a rackmount, (c) the complete system including the computer.

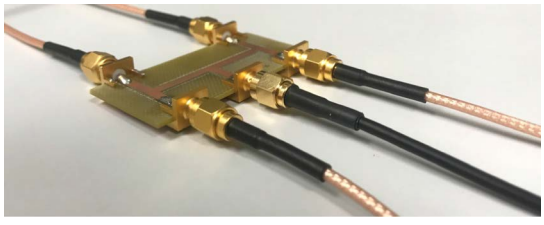

FIGURE 5. Four-way power divider used for phase synchronization of the SDR Array.

For brevity, we only summarize our receive calibration process. Each device measures the reference signal phase and

amplitude from the power divider then makes corrections in software. We use correction factors calculated by recording N samples of the reference signal at each SDR over 100 ms. The array output forms a complex sample matrix $\boldsymbol{x}$ with elements x_{ij}, where j corresponds to the array element and i corresponds to the sample number. The resulting correction factors are

$$c_i = \frac{1}{N}\sum_{i=0}^{N-1}\frac{x_{i0}}{x_{ij}}, \tag{5}$$

where c_i is the complex correction factor for the j^{th} element.

We experimentally verified the calibration processes by measuring the phase and amplitude received by each SDR from a fifth NI USRP-2922 that transmitted a calibration signal. The transmitting USRP was connected to the Octoclock, so its LO frequency and sample times were matched to those of the array SDRs. To ensure that the receiver measures the transmitted signal, the transmitted signal frequency was increased by 1 kHz. This frequency offset was removed from the received signals in software [50].

The transmitting SDR delivered a continuous wave signal with a predictable amplitude and phase to each SDR in the array. The amplitudes and phases of the beamformer SDRs before and after calibration are shown in a polar plot in Fig. 6. The amplitude scales and phases of these graphs are normalized so the first array element has a unit amplitude and zero phase. We note that the amplitudes are nearly equal before calibration, but the phases are not. Consequently, only phase calibration is critical for coherent beamforming. Similar results were observed when calibrating the beamformer for transmission.

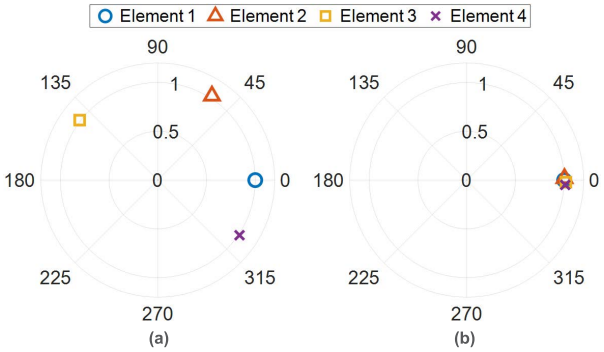

FIGURE 6. Time-dependent amplitude and phase data received by the SDR array, (a) before calibration, (b) after calibration.

C. DATA ACQUISITION SOFTWARE

A LabVIEW virtual instrument (VI) calibrates the array before measuring the SINR. The VI then loops over test conditions, which include a list of interferer power settings. During each test case, the interference cancellation algorithm calculates the array weights once then the VI measures the SINR. To provide a visual representation of the impact of interference on a digital transmission, a separate pair of transmit/receive programs measure constellation patterns and receive image data. The transmitter program sends a digital signal with a specified modulation scheme, carrier frequency, and symbol rate. This transmitter sends a 10 KiB pseudorandom digital noise signal or an image file as an uncompressed bitmap. The SDR array applies the array weights from interference cancellation algorithms in each measurement. After measuring a signal, the receiver generates constellation plots for the signal or exports the data to a file, including exporting a received uncompressed bitmap image transmission as a JPEG file. A screenshot of the receiver interface appears in Fig. 7.

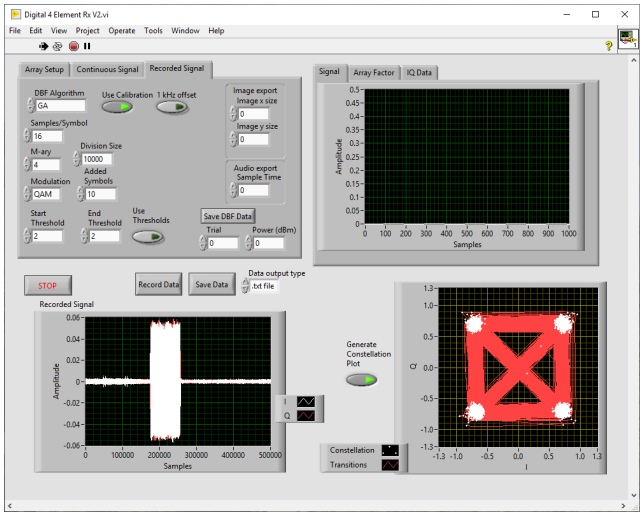

FIGURE 7. Screenshot of the digital receiver program in NI LabVIEW.

IV. EXPERIMENTAL STUDIES ON ADAPTIVE NULLING USING CONVENTIONAL ALGORITHMS

Array processing enhances the reception (or detection) of a desired signal in an environment containing numerous interference signals. Adaptive nulling algorithms place nulls in the directions of interference sources in order to maximize the system SINR. In this section we study the performance of conventional adaptive nulling algorithms using our experimental testbed.

A. EXPERIMENTAL SETUP AND MEASUREMENTS

Our experiments use one USRP to transmit 4-QAM digital data to the four-element beamformer described in Section II. The transmitter is placed broadside of the array at a distance of approximately 4 meters. A Signal Hound VSG25A vector signal generator placed approximately at a 45° angle from broadside and at a distance of 2 meters generates interference. The experiments take place on lab benches (Fig. 4), not an anechoic chamber, and we note that multiple large reflecting objects such as file cabinets, desks, etc. in close vicinity of the setup create a realistic environment for indoor wireless communications.

We averaged the SINRs over 16 independent trials. The measurements started with a calculation of the array weighting vector for each interference cancellation algorithm using a 2.45 GHz continuous-wave (CW) signal from the transmitting SDR and 1 KHz square wave from the interference generator. The SDR array recorded the received signal, then each interference cancellation algorithm separately calculated array weights using the same recorded signal in order to have a fair comparison. SINRs are computed using separate measurements of background noise and CW signals from the transmitter and interferer to approximate the ratio of the measured transmitter power to the sum of interference and noise power. Each power level is calculated by applying an interference cancellation weighting vector to the relevant recorded signal and calculating the squared mean amplitude of the resulting weighted signal.

B. ADAPTIVE NULLING EXPERIMENTS WITH SYNCHRONIZED BEAMFORMERS

The experiments reported in this section have the transmitter interfacing to the array Octoclock in order to synchronize the transmit and receive LO frequencies and remove any carrier frequency offset between the two devices. These experiments serve as a basis for comparing the interference cancellation algorithms in an ideal situation.

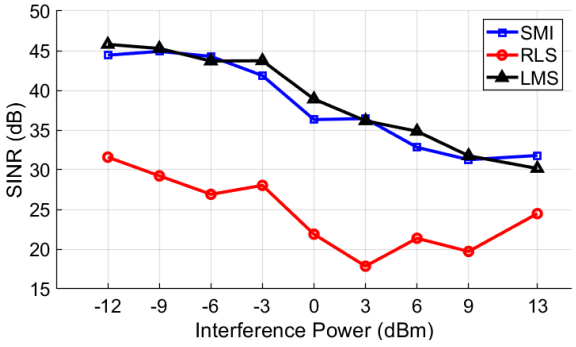

FIGURE 8. Measured SINR as a function of interference power for SMI, RLS, and LMS algorithms.

Fig. 8 displays plots of average SINR over 16 trials. SMI and LMS maintain SINRs above 30 dB for all interferer power levels. RLS underperforms LMS and SMI despite an expectation that it would show similar performance to SMI. This is likely related to the square wave interference used in interference cancellation weight calculations. RLS is a nonstationary algorithm that loops over all recorded time samples and, in each iteration, considers both current and previous time samples in estimating the array weighting vector. This may reduce its ability to adapt to sudden changes in the interfering signal such as those seen with square wave interference. Increasing the time constant α in RLS such that multiple cycles of the interfering signal are considered may improve this performance. Despite some issues with the RLS algorithm, all three beamforming algorithms were able to effectively cancel the interference and dramatically improve the SINR. The received constellation graphs for a single trial appear in Fig. 9. Note that the received signal for the uniform array is completely corrupted, but the DBF algorithms successfully cancel the interference and receive the 4-QAM signal.

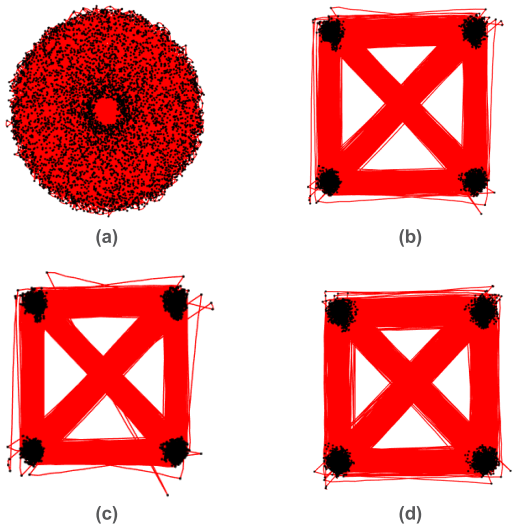

FIGURE 9. Constellation plots for the received 4-QAM with: (a) uniform weights, (b) LMS weights, (c) SMI weights, and (d) RLS weights.

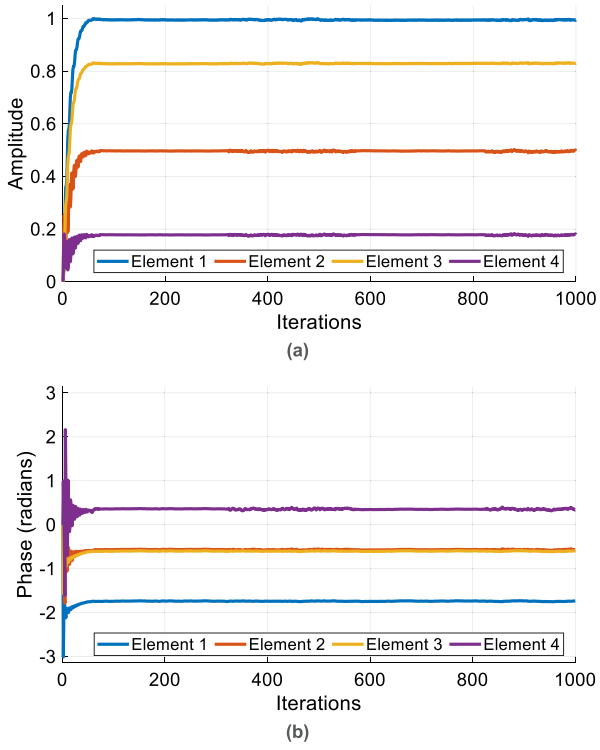

FIGURE 10. Measured conversion graphs for the beamformer element weights using the LMS algorithm: (a) amplitude, (b) phase.

Finally, in this section we provide graphs showing the convergence of the weights from the iterative algorithms.

Measured conversion graphs for the LMS algorithm are given in Fig. 10. Similar results were observed for the RLS algorithm. In the experiments conducted, these algorithms typically converged with less than 100 iterations.

V. ROBUST ADAPTIVE NULLING WITH NOVEL ALGORITHMS

In Section IV the transmitter and receiver were synchronized. In a realistic scenario, however, there is a carrier frequency offset between the transmitter and receiver. This carrier offset shifts the frequency of the signal output from the digital beamformer and prevents it from matching the expected signal in the interference cancellation algorithms. Here we present two new adaptive nulling approaches that are robust to carrier frequency offset, i.e., they operate without the need to synchronize the transmitter and receiver.

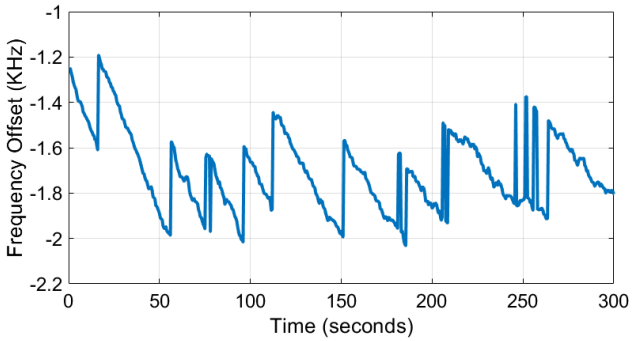

FIGURE 11. Measured carrier frequency offset of the transmitter versus time.

The measured carrier frequency offset of the transmitter over a period of five minutes is shown in Fig. 11. We note that a control loop ensures that the carrier frequency offset variation remains within a desired range for the transmitter. This frequency offset appears as a progressive increase or decrease in the complex phase of the signal, which can be expressed by $X_{nm} \rightarrow X_{nm}e^{j\Delta\omega n}$ for a carrier frequency offset of $\Delta\omega$. In turn, the signal vector is replaced by $s_n \rightarrow s_n e^{j\Delta\omega n}$. The frequency offset reduces the correlation between the received signal from the target device with the expected reference signal, meaning non-robust interference cancellation algorithms typically try to null the intended transmitter in order to minimize the mean square error cost function in (3). The resulting SINRs are shown in Fig. 12. Disconnecting the SDR transmitter from the array Octoclock offsets the transmitter carrier frequency from the receiver carrier frequency by a few kilohertz.

The carrier frequency offset significantly reduces the performance of the SMI, RLS, and LMS algorithms. The SMI algorithm proves to be the most sensitive, because SMI requires a high correlation between the entire received and expected reference signals, as opposed to measuring correlation over a narrower time period such as in LMS and RLS algorithms. The LMS algorithm, on the other hand, shows a much better robustness to carrier offsets, since it uses only one time sample at each iteration, so the received signal phase change is small. While the trend is similar in RLS, due to its nonstationary iterative approach, it is more sensitive to these offsets in comparison with LMS. Nonetheless, the performance of all three algorithms significantly degrades when carrier frequency offsets are not accounted for, and none of the algorithms converge.

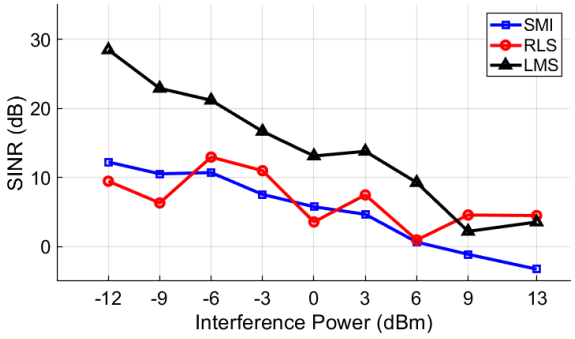

FIGURE 12. Measured SINR as a function of interference power for SMI, RLS, and LMS algorithms without transmitter synchronization.

One potential solution measures and corrects for this offset before performing interference cancellation. However, high-interference and high-multipath environments typically preclude measuring the intended signal so, determining the carrier frequency offset may not be feasible. Robust interference cancellation thus requires algorithms that remove corruptions, such as carrier frequency offsets, in the signal. The most widely adopted solution to beamformer mismatch problems is diagonal loading and equivalent approaches [18]–[22]. These techniques provide robustness by effectively designing for a higher white noise level than is actually present. To mitigate some of these issues, variable loading has more recently been introduced; it improves robustness to steering vector errors while maintaining a desired SINR. While these techniques can provide robustness to certain mismatch issues, and usually at the expense of a higher noise, to the best of our knowledge, very limited work has been reported on robust approaches that account for signal corruptions arising from carrier frequency offsets [17], [23], [24]. Our studies in this section investigates new techniques that provide robustness without adding noise to the system, i.e., beamforming with maximum SINR.

A. AMPLITUDE-ONLY ALGORITHMS

Since carrier frequency offsets appear as progressive phase shifts in the signal, the robust algorithms proposed here ignore signal phase and perform amplitude-only optimization of the array weighting vector. In this case, the elements in the received signal and the expected reference signal have amplitudes but no phases. Fig. 13 shows the SINR performance of amplitude-only SMI (AOSMI), amplitude-only LMS (AOLMS), and amplitude-only RLS (AORLS) vs. interference power. Amplitude-only algorithms outperform conventional algorithms when a carrier frequency offset is

present. This can be seen by comparing the SINR graphs in Figs. 12 and 13, where amplitude-only approaches achieve an SINR above 20 dB at the lower interference power levels. It is also important to note that amplitude-only approaches have nearly identical performance with or without synchronization. However, these approaches produce real-valued array weighting vectors. In order to cancel interference, the amplitudes of the interfering and received signals must vary between the array elements. In a high multipath environment, such as the lab used for our measurements, multipath effects provide the spatial diversity needed for amplitude-only optimization. It is also important to note that, a real-valued array weighting vector cannot steer the array's main beam, so a separate phase shift must be applied in order to scan the beam.

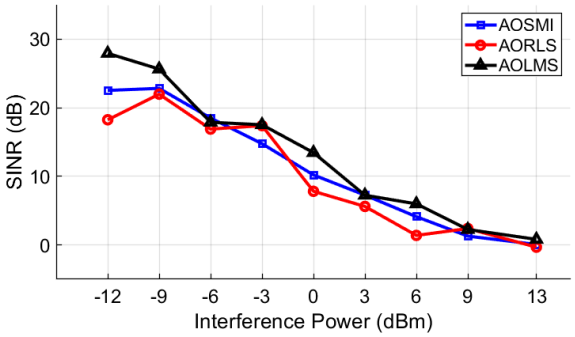

FIGURE 13. Measured SINR as a function of interference power for the new amplitude-only algorithms without transmitter synchronization.

B. EVOLUTIONARY ALGORITHMS

A better approach to interference cancellation in the presence of carrier frequency offsets can be implemented by designing an interference cancellation cost function that is more robust to these offsets. The new fitness function proposed in this work is

$$\text{cost} = \| |d(t)| - |wx(t)| \|_{\infty} . \tag{6}$$

Here $|.|$ denotes an element-wise modulus and the l_{∞} norm returns the modulus of the largest input vector element. The l_{∞} norm improves performance when interference occurs in short bursts. The element-wise moduli in (6) removes phase data from the signals. An important difference between (6) and (2), i.e., the error vector in conventional techniques, is that the element-wise modulus of the received signal occurs after summing all of the element signals. This new interference cancellation cost function requires the reference signal to have a different amplitude profile than the interference, which is the case in a high multipath environment. This new cost function also presents a more challenging optimization problem and requires a nonconvex search algorithm. Here, we implement a genetic algorithm (GA) to minimize this cost function, although other evolutionary algorithms work well for this purpose too.

The GA algorithm outperforms all other algorithms, including the new amplitude-only methods, when the

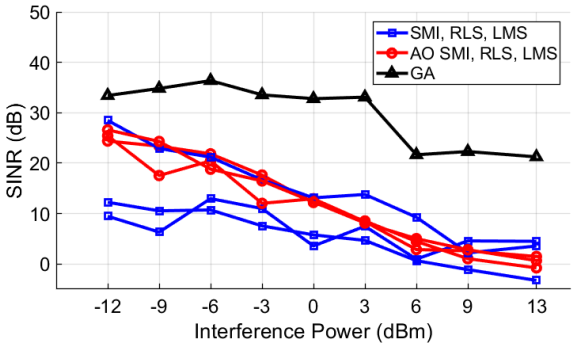

FIGURE 14. Measured SINR as a function of interference power for the seven algorithms: conventional approaches, new amplitude-only approaches, and new GA approach without transmitter synchronization.

transmitter and received are not synchronized and a carrier frequency offset exists as shown in Fig. 14. A qualitative comparison using image data is also performed. Fig. 15 compares the performance of the GA algorithm and AOSMI, when the transmitter sent uncompressed image data to the receiver array while the interferer sent an interfering CW signal at −6 dBm. We note that in this experiment, the conventional SMI algorithm fails to recover the image. The AOSMI however reproduces an image with some distortion, while the GA algorithm reproduces the image with little error.

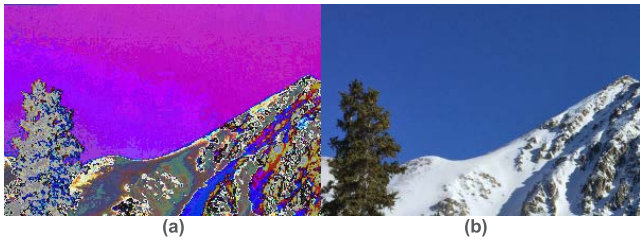

FIGURE 15. Received images in the presence of interference using interference cancellation weight from: (a) AOSMI and (b) GA. The transmitter was not synchronized to the receiver in either case.

Carrier frequency offset negatively impacts the performance of wireless communication systems. The studies conducted here show that if these offsets cannot be measured a priori, then algorithms need to be robust to the resulting signal corruption. We show that conventional adaptive nulling algorithms such as LMS, SMI, and RLS do not converge and fail to cancel interference sources when frequency offsets are not accounted for. Here we propose two solutions to this problem. The first approach uses the conventional algorithms, but ignores signal phase, essentially performing an amplitude-only optimization of the array weighting vector. The experimental results show that this approach provides a much higher SINR than conventional algorithms and is capable of interference cancelation in the presence of carrier frequency offsets (see Fig. 14). We also present a second approach that is based on a new interference cancellation error function and uses an evolutionary search algorithm (GA in our studies) for the problem. We show that this approach

is also capable of interference cancellation in the presence of carrier frequency offsets. Our experimental studies showed that in comparison between the two proposed algorithms, the GA approach provides a higher SINR and is more effective for adaptive interference cancelation in high-multipath and high-interference environments.

VI. CONCLUSION

We experimentally demonstrate a low-cost platform for DBF using an array of software defined radios. We describe the hardware architecture of the in-house developed beamformer along with experimental results on adaptive interference cancellation. Furthermore, we highlight some limitations of conventional beamforming algorithms and experimentally show that when carrier frequency offsets cannot be measured and corrected, these algorithms will fail. We then propose two solutions to this problem and experimentally demonstrate the robustness of our approaches. The experimental results presented show our proposed techniques provides robustness to this type of signal corruption without degrading SINR or other system performance factors.

ACKNOWLEDGMENT

The authors would like to thank Igor Alvarado and Haydn Nelson from the National Instruments for their technical advice and continued support throughout this research. They also wish to thank the reviewers whose thoughtful comments greatly helped to improve the quality and efficacy of this manuscript.

REFERENCES

[1] Z. Li, Y. Liu, K. G. Shin, J. Liu, and Z. Yan, "Interference steering to manage interference in IoT," *IEEE Internet Things J.*, vol. 6, no. 6, pp. 10458–10471, Dec. 2019.

[2] L. Chettri and R. Bera, "A comprehensive survey on Internet of Things (IoT) toward 5G wireless systems," *IEEE Internet Things J.*, vol. 7, no. 1, pp. 16–32, Jan. 2020.

[3] B. Widrow, P. E. Mantey, L. J. Griffiths, and B. B. Goode, "Adaptive antenna systems," *Proc. IEEE*, vol. 55, no. 12, pp. 2143–2159, Dec. 1967.

[4] H. L. Van Trees, *Optimum Array Processing: Part IV of Detection, Estimation, and Modulation Theory*. Hoboken, NJ, USA: Wiley, 2002.

[5] R. L. Haupt, *Antenna Arrays: A Computational Approach*. Hoboken, NJ, USA: Wiley, 2010.

[6] R. A. Monzingo, R. L. Haupt, and T. W. Miller, *Introduction to Adaptive Antennas*, 2nd ed. Rijeka, Croatia: SciTech, 2011.

[7] H. Steyskal, "Digital beamforming at Rome laboratory," *Microw. J.*, vol. 39, pp. 100–124, Feb. 1996.

[8] L. Pettersson, M. Danestig, and U. Sjostrom, "An experimental S-band digital beamforming antenna," *IEEE Aerosp. Electron. Syst. Mag.*, vol. 12, no. 11, pp. 19–29, Nov. 1997.

[9] L. Sun, Y. Qin, Z. Zhuang, R. Chen, Y. Zhang, J. Lu, F. Shu, and J. Wang, "A robust secure hybrid analog and digital receive beamforming scheme for efficient interference reduction," *IEEE Access*, vol. 7, pp. 22227–22234, 2019.

[10] D. Zhang, J. Zhang, C. Cui, W. Wu, and D. Fang, "Single RF channel digital beamforming array antenna based on compressed sensing for large-scale antenna applications," *IEEE Access*, vol. 6, pp. 4340–4351, 2018.

[11] M.-C. Hua, C.-H. Hsu, and H.-C. Liu, "Implementation of direction-of-arrival estimator on software defined radio platform," in *Proc. 8th Int. Symp. Commun. Syst., Netw. Digit. Signal Process. (CSNDSP)*, Jul. 2012, pp. 1–4.

[12] A. Akindoyin, M. Willerton, and A. Manikas, "Localization and array shape estimation using software defined radio array testbed," in *Proc. IEEE 8th Sensor Array Multichannel Signal Process. Workshop (SAM)*, Jun. 2014, pp. 189–192.

[13] C. Campo, M. Stefer, L. Bernard, S. Hengy, H. Boeglen, and J. M. Paillot, "Antenna weighting system for a uniform linear array based on software defined radio," in *Proc. Medit. Microw. Symp. (MMS)*, Nov. 2017, pp. 1–4.

[14] P. Nayeri and R. L. Haupt, "A testbed for adaptive beamforming with software defined radio arrays," in *Proc. IEEE/ACES Int. Conf. Wireless Inf. Technol. Syst. (ICWITS) Appl. Comput. Electromagn. (ACES)*, Mar. 2016, pp. 1–2.

[15] D. Gaydos, P. Nayeri, and R. Haupt, "Experimental demonstration of a software-defined-radio adaptive beamformer," in *Proc. 15th Eur. Radar Conf. (EuRAD)*, Sep. 2018, pp. 561–564.

[16] D. Gaydos, P. Nayeri, and R. L. Haupt, *Experimental Comparison of Digital Beamforming Interference Cancellation Algorithms Using a Software Defined Radio Array*. Boulder, CO, USA: URSI Boulder, Jan. 2019.

[17] D. Gaydos, P. Nayeri, and R. Haupt, "Adaptive beamforming in high-interference environments using a software-defined radio array," in *Proc. IEEE Int. Symp. Antennas Propag. USNC-URSI Radio Sci. Meeting*, Jul. 2019, pp. 1501–1502.

[18] M. W. Ganz, R. L. Moses, and S. L. Wilson, "Convergence of the SMI and the diagonally loaded SMI algorithms with weak interference (adaptive array)," *IEEE Trans. Antennas Propag.*, vol. 38, no. 3, pp. 394–399, Mar. 1990.

[19] R. L. Dilsavor and R. L. Moses, "Analysis of modified SMI method for adaptive array weight control," *IEEE Trans. Signal Process.*, vol. 41, no. 2, pp. 721–726, Feb. 1993.

[20] J. Gu, "Robust beamforming based on variable loading," *Electron. Lett.*, vol. 41, no. 2, pp. 55–56, Jan. 2005.

[21] X. Li, D. Wang, X. Ma, and Z. Xiong, "Robust adaptive beamforming using iterative variable loaded sample matrix inverse," *Electron. Lett.*, vol. 54, no. 9, pp. 546–548, May 2018.

[22] L. Yu, W. Liu, and R. Langley, "SINR analysis of the subtraction-based SMI beamformer," *IEEE Trans. Signal Process.*, vol. 58, no. 11, pp. 5926–5932, Nov. 2010.

[23] S. Li, D. Gaydos, P. Nayeri, and M. B. Wakin, "Adaptive interference cancellation using atomic norm minimization and denoising," *IEEE Antennas Wireless Propag. Lett.*, vol. 19, no. 12, pp. 2349–2353, Dec. 2020.

[24] J. Chuang, J. Senic, C. Liu, C. Gentile, S. Y. Jun, and D. Caudill, "Blind calibration of phase drift in millimeter-wave channel sounders," *IEEE Access*, vol. 8, pp. 109557–109567, 2020.

[25] R. C. Hansen, *Phased Array Antennas*, 2nd ed. Hoboken, NJ, USA: Wiley, 2009.

[26] R. J. Mailloux, *Phased Array Antenna Handbook*, 3rd ed. Norwood, MA, USA: Artech House, 2017.

[27] A. K. Bhattacharyya, "Phased array fundamentals: Pattern analysis and synthesis," in *Phased Array Antennas: Floquet Analysis Synthesis BFNs and Active Array Systems*. Hoboken, NJ, USA: Wiley, 2006.

[28] T. S. Rappaport, S. Sun, R. Mayzus, H. Zhao, Y. Azar, K. Wang, G. N. Wong, J. K. Schulz, M. Samimi, and F. Gutierrez, "Millimeter wave mobile communications for 5G cellular: It will work!" *IEEE Access*, vol. 1, pp. 335–349, 2013.

[29] S. Rangan, T. S. Rappaport, and E. Erkip, "Millimeter-wave cellular wireless networks: Potentials and challenges," *Proc. IEEE*, vol. 102, no. 3, pp. 366–385, Mar. 2014.

[30] J. Ala-Laurinaho, J. Aurinsalo, A. Karttunen, M. Kaunisto, A. Lamminen, J. Nurmiharju, A. V. Räisänen, J. Säily, and P. Wainio, "2-D beam-steerable integrated lens antenna system for 5G E-band access and backhaul," *IEEE Trans. Microw. Theory Techn.*, vol. 64, no. 7, pp. 2244–2255, Jul. 2016.

[31] R. Garg and A. S. Natarajan, "A 28-GHz low-power phased-array receiver front-end with 360° RTPS phase shift range," *IEEE Trans. Microw. Theory Techn.*, vol. 65, no. 11, pp. 4703–4714, Nov. 2017.

[32] K. Kibaroglu, M. Sayginer, and G. M. Rebeiz, "A quad-core 28–32 GHz transmit/receive 5G phased-array IC with flip-chip packaging in SiGe BiCMOS," in *IEEE MTT-S Int. Microw. Symp. Dig.*, Jun. 2017, pp. 1892–1894.

[33] R. L. Haupt and H. L. Southall, "Experimental adaptive nulling with a genetic algorithm," *Microw. J.*, vol. 42, no. 1, pp. 78–89, Jan. 1999.

[34] P. Nayeri and R. Haupt, "A comparison of digital beamforming and power minimization adaptive nulling algorithms using a software defined radio antenna array," in *Proc. IEEE Int. Symp. Antennas Propag. USNC/URSI Nat. Radio Sci. Meeting*, Jul. 2018, pp. 7–8.

[35] D. Sikri and R. M. Jayasuriya, "Multi-beam phased array with full digital beamforming for SATCOM and 5G," *Microw. J.*, vol. 62, no. 4, pp. 64–79, Apr. 2019.

[36] P. K. Bailleul, "A new era in elemental digital beamforming for spaceborne communications phased arrays," *Proc. IEEE*, vol. 104, no. 3, pp. 623–632, Mar. 2016.
[37] B. Yang, Z. Yu, J. Lan, R. Zhang, J. Zhou, and W. Hong, "Digital beamforming-based massive MIMO transceiver for 5G millimeter-wave communications," *IEEE Trans. Microw. Theory Techn.*, vol. 66, no. 7, pp. 3403–3418, Jul. 2018.
[38] W. Roh, J. Y. Seol, J. Park, B. Lee, J. Lee, Y. Kim, J. Cho, K. Cheun, and F. Aryanfar, "Millimeter-wave beamforming as an enabling technology for 5G cellular communications: Theoretical feasibility and prototype results," *IEEE Commun. Mag.*, vol. 52, no. 2, pp. 106–113, Feb. 2014.
[39] S. B. Venkatakrishnan, D. K. Papantonis, A. A. Akhiyat, E. A. Alwan, and J. L. Volakis, "Experimental validation of on-site coding digital beamformer with ultra-wideband antenna arrays," *IEEE Trans. Microw. Theory Techn.*, vol. 65, no. 11, pp. 4408–4417, Nov. 2017.
[40] T. E. Bogale, L. B. Le, A. Haghighat, and L. Vandendorpe, "On the number of RF chains and phase shifters, and scheduling design with hybrid analog-digital beamforming," *IEEE Trans. Wireless Commun.*, vol. 15, no. 5, pp. 3311–3326, May 2016.
[41] L. Zhu, J. Zhang, Z. Xiao, X. Cao, D. O. Wu, and X.-G. Xia, "3-D beamforming for flexible coverage in millimeter-wave UAV communications," *IEEE Wireless Commun. Lett.*, vol. 8, no. 3, pp. 837–840, Jun. 2019.
[42] S. Dutta, C. N. Barati, D. Ramirez, A. Dhananjay, J. F. Buckwalter, and S. Rangan, "A case for digital beamforming at mmWave," *IEEE Trans. Wireless Commun.*, vol. 19, no. 2, pp. 756–770, Feb. 2020.
[43] A. M. Wyglinski, D. P. Orofino, M. N. Ettus, and T. W. Rondeau, "Revolutionizing software defined radio: Case studies in hardware, software, and education," *IEEE Commun. Mag.*, vol. 54, no. 1, pp. 68–75, Jan. 2016.
[44] J. Liu, W. Liu, H. Liu, B. Chen, X.-G. Xia, and F. Dai, "Average SINR calculation of a persymmetric sample matrix inversion beamformer," *IEEE Trans. Signal Process.*, vol. 64, no. 8, pp. 2135–2145, Apr. 2016.
[45] I. P. Gravas, Z. D. Zaharis, T. V. Yioultsis, P. I. Lazaridis, and T. D. Xenos, "Adaptive beamforming with sidelobe suppression by placing extra radiation pattern nulls," *IEEE Trans. Antennas Propag.*, vol. 67, no. 6, pp. 3853–3862, Jun. 2019.
[46] *NI USRP-292x/293x Datasheet*. Accessed: Aug. 16, 2021. [Online]. Available: http://www.ni.com/datasheet/pdf/en/ds-355
[47] *Laboratory Virtual Instrument Engineering Workbench*, National Instruments, Austin, TX, USA, 2020.
[48] *OctoClock-G CDA-2990 Datasheet*. Accessed: Aug. 16, 2021. [Online]. Available: https://www.ettus.com/content/files/Octoclock_Spec_Sheet.pdf
[49] *VSG25A Vector Signal Generator Datasheet*. Accessed: Aug. 16, 2021. [Online]. Available: https://signalhound.com/products/vsg25a-vector-signal-generator/
[50] J. G. Proakis and D. K. Manolakis, *Digital Signal Processing*, 4th ed. London, U.K.: Pearson, 2006.

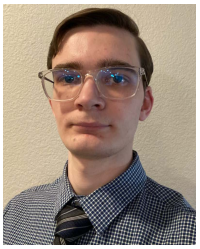

DANIEL CHRISTOPHER GAYDOS received the Bachelor of Science degree in engineering physics and the Master of Science degree in electrical engineering from the Colorado School of Mines, Golden, CO, USA, in 2018 and 2020, respectively.

He is currently a Former Student of the Colorado School of Mines. He is also employed at Zeta Associates, Aurora, CO, USA, as a Software Engineer. His former occupations include an internship at Zeta Associates and employment as a Research Assistant at the Colorado School of Mines. His research interest includes smart antennas.

Mr. Gaydos was a recipient of the 2019 MTT-S Graduate Microwave Engineering Fellowship Award, an Honorable Mention in the 2019 AP-S Student Paper Competition, and the 2019 NRSM Travel Fellowship.

PAYAM NAYERI (Senior Member, IEEE) received the B.Sc. degree in applied physics from Shahid Beheshti University, Tehran, Iran, in 2004, the M.Sc. degree in electrical engineering from the Iran University of Science and Technology, Tehran, in 2007, and the Ph.D. degree in electrical engineering from the University of Mississippi, University, MS, USA, in 2012.

He is currently an Assistant Professor with the Department of Electrical Engineering, Colorado School of Mines. He is the lead author of the book *Reflectarray Antennas: Theory, Designs, and Applications* (Wiley-IEEE Press, 2018). He has authored/coauthored over 95 journal articles and conference papers. His research interests include applied electromagnetics with a focus on phased-array antennas, digital arrays and array processing, artificial intelligence techniques for synthesis of antennas and arrays, reflectarrays and array lenses, and intelligent electromagnetic surfaces.

Prof. Nayeri is a member of Sigma Xi and Phi Kappa Phi. He was a recipient of several prestigious awards, including the IEEE Antennas and Propagation Society Doctoral Research Award in 2010, the University of Mississippi Graduate Achievement Award in Electrical Engineering in 2011, and the 2021 Electrical Engineering Excellence in Teaching Award at the Colorado School of Mines. Since 2019, he has been serving as an Associate Editor for the IEEE Antennas and Wireless Propagation Letters.

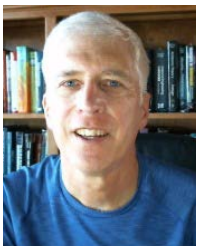

RANDY L. HAUPT (Life Fellow, IEEE) received the M.S. degree in engineering management from the Western New England College, the M.S.E.E. degree from Northeastern University, and the Ph.D. degree in EE from the University of Michigan.

He was a Project Engineer with the OTH-B radar and a Research Antenna Engineer with the Rome Air Development Center. He has a BSEE USAF Academy. He was a Professor and the Department Head at Colorado School of Mines, an RF Staff Consultant at Ball Aerospace & Technologies, Corporation, a Senior Scientist and the Department Head at the Applied Research Laboratory of Penn State, a Professor and the Department Head of ECE at Utah State, a Professor and the Chair of EE at the University of Nevada Reno, and a Professor of EE at the USAF Academy. He currently works as a Consultant. He coauthored *Practical Genetic Algorithms*, 2nd edition, 2004, *Genetic Algorithms in Electromagnetics*, 2007, and *Introduction to Adaptive Antennas*, 2010. He authored *Antenna Arrays: A Computation Approach*, 2010, *Timed Arrays: Wideband and Time Varying Antenna Arrays*, 2015, and *Wireless Communications Systems: An Introduction*, 2020.